Optical Engineering

OpticalEngineering.SPIEDigitalLibrary.org

Sinusoidal Siemens star spatial frequency response measurement errors due to misidentified target centers

Gabriel C. Birch
John C. Griffin

SPIE.

Sinusoidal Siemens star spatial frequency response measurement errors due to misidentified target centers

Gabriel C. Birch* **and John C. Griffin**
Sandia National Laboratories, P.O. Box 5800 MS 0781, Albuquerque, New Mexico 87185, United States

Abstract. Numerous methods are available to measure the spatial frequency response (SFR) of an optical system. A recent change to the ISO 12233 photography resolution standard includes a sinusoidal Siemens star test target. We take the sinusoidal Siemens star proposed by the ISO 12233 standard, measure system SFR, and perform an analysis of errors induced by incorrectly identifying the center of a test target. We show a closed-form solution for the radial profile intensity measurement given an incorrectly determined center and describe how this error reduces the measured SFR of the system. Using the closed-form solution, we propose a two-step process by which test target centers are corrected and the measured SFR is restored to the nominal, correctly centered values. [DOI: 10.1117/1.OE.54.7.074104]

Keywords: spatial frequency response; modulation transfer function; resolution; image quality evaluation; Siemens star.

Paper 150631 received May 14, 2015; accepted for publication Jun. 29, 2015; published online Jul. 23, 2015.

1 Introduction

Measuring the spatial frequency response (SFR) of an optical system remains an intricate task, with several test methodologies available to the optical scientist and engineer, including slanted edge tests and measurements from known noise targets. Modifications to the ISO 12233 photography resolution standard[1] in February, 2014, now include a sinusoidal Siemens star as an approved test target. Work has been conducted to compare the results of the sinusoidal Siemens star measurement to other techniques, such as edge-spread function measurements,[2,3] and the Siemens star target has been implemented as a useful test methodology in numerous applications for SFR measurements.[4–11] However, to the authors' knowledge, no error analysis of the SFR processing methods for imagery of a sinusoidal Siemens star has been conducted.

A piece of the total error analysis for this process has been conducted by investigating the errors due to inaccurate center identification, and several findings are presented. The mathematical function for the measured intensity of a sinusoidal Siemens star target with an incorrectly determined center location is derived and shown to cause effective changes to the sampled spatial frequency of the sinusoidal Siemens star target. Small pixel shifts in the center location are shown to induce significant degradation in the measured SFR compared to the nominal, correctly centered measurements. Mitigation of the errors introduced by incorrectly determined centers through increasing angular segmentation of the star target is discussed, and it is shown that imagers with a better resolution performance (i.e., higher SFR) suffer more from incorrectly determined centers than an equivalent system with a worse performance. Finally, the use of a two-step process whereby centers are coarsely found then corrected with the closed-form definition is demonstrated with a Monte-Carlo simulation. Postcorrected SFR measurements are shown to produce results consistent with correctly centered targets for both simulated imagery and real images from a digital camera.

This document begins by discussing the generalized process for measuring the SFR of an optical system from the image of a sinusoidal Siemens star target. A mathematical analysis of measured intensity values given a sinusoidal Siemens star target with an incorrectly determined center is then discussed. The effects from sampling and optical aberration are introduced and compared to the mathematical results. Target segmentation and its effect on measured SFR are then examined. The mitigation of incorrectly found centers is then detailed using the derived mathematical definition. Finally, the results are summarized and future areas of investigation are proposed.

2 Siemens Stars and Spatial Frequency Response Measurements

A sinusoidal Siemens star is comprised of sinusoidal oscillations in a polar coordinate system such that the spatial frequency varies for concentric circles of different sizes. This pattern, displayed in Fig. 1, is defined as

$$I(\theta) = a + b\,\sin(\omega\theta - \phi), \tag{1}$$

where the intensity I is described by a sinusoidal function of the polar angle θ. In addition, constants a, b, ω, and ϕ represent the mean intensity value, the amplitude of the intensity oscillations, the integer number of cycles within the complete 2π radians of the star, and a potential phase offset ($\phi = 0$ for all examples in this document), respectively. Note that in Eq. (1), the intensity is not a function of the radius r. However, the spatial frequency, ξ, is inversely proportional to the radius via the equation

$$\xi = \frac{\omega}{2\pi r}.$$

Given that ω is constant for a single star, the spatial frequency of a concentric sampled circle increases as the radius

*Address all correspondence to: Gabriel C. Birch, E-mail: gcbirch@sandia.gov

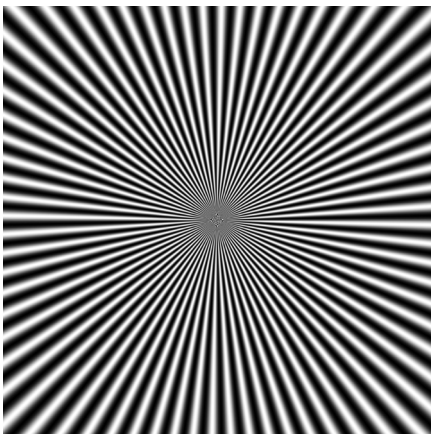

Fig. 1 Sinusoidal Siemens star target as defined by Eq. (1).

of that circle decreases, thereby allowing for a wide spectrum of spatial frequencies between the minimum and maximum radii of the star.

Contrary to this ideal definition, an actual captured image of the sinusoidal Siemens star is influenced by many real-world factors that affect the intensity of the image, especially as a function of spatial frequency. A few of these influential factors include a nonideal performance due to optical aberration, sampling effects, and image postprocessing. Therefore, the actual image response for various spatial frequencies is desired. This is accomplished by an SFR measurement which determines image contrast across a range of radii within the imaged Siemens star.

The process by which images of a sinusoidal Siemens star are captured by a camera and SFR data is extracted has been discussed in the literature.[3,12] This process generally requires the steps that follow. First, an image is captured by the imaging system under test and regions of interest are identified within the image (i.e., target locations, fiducial markers, and so on). Once a Siemens star target has been identified and linearization of the intensity values has been performed, circular pixel profiles are extracted for a range of radii. This circular sampling of a rectangular pixel grid follows the "nearest" pixel value recommendation of the ISO 12233 standard, which essentially states that any pixel that the true circular profile passes through is included in the sampled profile. Hence, no interpolation is performed and only true pixel samples are used to evaluate the SFR. Each extracted profile is fit to the known sinusoidal function, and the contrast level is determined based on the known spatial frequency of the test target. This process is repeated for varying radii such that image contrast is measured as a function of spatial frequency. Division of the sinusoidal Siemens star target into angular wedges is often performed, typically called target segmentation. The purpose of segmentation is stated by the ISO document to mitigate local distortion within the region of the test chart. Segmentation also enables analysis of SFR at different angular directions (i.e., horizontal SFR versus vertical SFR), which can be a desirable analysis for certain applications. The ISO 12233 standard states the 8 segments are typically used, but this value is ultimately chosen by the user.

Because this investigation focuses on the fundamental errors associated with the analysis of an imaged sinusoidal Siemens star target, complicating factors are at first removed and later reintroduced. Initial analysis is done solely in the mathematics domain, using a mathematically defined sinusoidal Siemens target and extracting the entire radial profile for contrast determination (i.e., a single segment is used). Images of mathematically generated sinusoidal Siemens star targets are then examined, and the effects of image sampling and optical aberration are added to the analysis. The purpose of target segmentation is analyzed further and the optimal segment number is calculated. Finally, the use of a two-step process to correct for an incorrect center is demonstrated on both mathematically generated sinusoidal Siemens star targets, and an image from a digital camera.

3 Errors from Offset Center

In the ideal scenario, the center location of the Siemens star is determined and the image is sampled about the correct center. This ensures that each arc of constant radius is described by a single spatial frequency. However, accurately calculating the center coordinates of the star can be difficult, especially in the presence of image distortion or for a low-resolution image. Any center-finding algorithm is expected to perform with some error, and the extracted profiles from a sinusoidal Siemens star target with an incorrectly determined center will not exhibit pure sinusoidal oscillations. In this section we first show the mathematically derived closed-form solution for measured intensity given a sinusoidal Siemens star and an offset center. Next, we show how this offset center affects the SFR measurement. The importance of target segmentation is then discussed. Finally, use of the closed-form solution to correct for offset centers is proposed and demonstrated.

3.1 *Mathematics of Incorrectly Centered Targets*

The perfect sinusoidal Siemens star with a center at $r = 0$ is described by Eq. (1), but the measured profiles are not the same for an image with a misaligned center. The coordinate systems for the true and offset centers are diagrammed in Fig. 2.

To find the closed-form definition of the measured sinusoidal Siemens star with an arbitrary center offset, we begin with the parametric equations of a circle centered around the

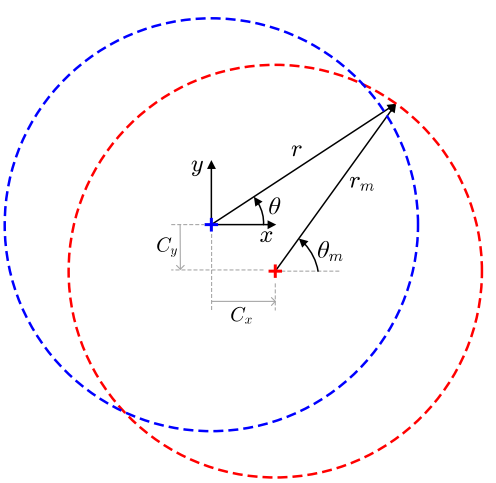

Fig. 2 Coordinate systems used to discuss correctly (blue) and incorrectly (red) determined centers for a sinusoidal Siemens star test target. In this diagram, $C_x > 0$ and $C_y < 0$.

offset center in order to easily translate between the two polar coordinate systems:

$$x = C_x + r_\mathrm{m}\cos\theta_\mathrm{m} \quad y = C_y + r_\mathrm{m}\sin\theta_\mathrm{m},$$

where r_m is the radius referenced from the offset center, θ_m is the polar angle, and C_x and C_y are the x and y center offsets in the Cartesian coordinate system, respectively. Given the parametric equations, the angle for an offset center circle relative to the true center is given by

$$\theta = \tan^{-1}\left(\frac{y}{x}\right) \quad = \tan^{-1}\left(\frac{C_y/r_\mathrm{m} + \sin\theta_\mathrm{m}}{C_x/r_\mathrm{m} + \cos\theta_\mathrm{m}}\right). \tag{2}$$

Figure 3 shows the relationship between the assumed angle for no center offset (θ_m) and the actual angle (θ) due to various offset centers. Because the polar angle is 2π periodic, an offset center modulates θ with various degrees of severity due to the magnitude of the offset.

The actual sampling angle in the case of an offset center [Eq. (2)] is substituted into Eq. (1), yielding the equation for the offset sinusoidal Siemens star

$$I(r_\mathrm{m},\theta_\mathrm{m}) = a + b\sin\left[\omega\tan^{-1}\left(\frac{C_y/r_\mathrm{m} + \sin\theta_\mathrm{m}}{C_x/r_\mathrm{m} + \cos\theta_\mathrm{m}}\right) - \phi\right]. \tag{3}$$

This equation reflects the impact of a constant offset center on the extracted intensity values and the introduction of a radial dependence that is due to the offset alone. Therefore, any circular profile extracted from an image of a sinusoidal Siemens star target with an incorrectly found center will not yield a pure sinusoidal profile, but rather a more complex sinusoidal profile modulated with an inverse tangent component. Furthermore, the deviation from a pure sinusoidal function increases nonlinearly as the radius of the extracted profile decreases, as shown in Fig. 3. Restated, this effect is much stronger at high-spatial frequencies than at low-spatial frequencies.

Because of the modulation in the θ, the effective angular frequency, denoted as ω_m, for a circular profile extracted for an offset center also exhibits a one cycle modulation. The effective angular frequency of Eq. (3) is calculated as

$$\omega_\mathrm{m} = \frac{\partial(\omega\theta - \phi)}{\partial\theta_\mathrm{m}} = \omega\frac{C_x r_\mathrm{m}\cos\theta_\mathrm{m} + C_y r_\mathrm{m}\sin\theta_\mathrm{m} + r_\mathrm{m}^2}{(C_x + r_\mathrm{m}\cos\theta_\mathrm{m})^2 + (C_y + r_\mathrm{m}\sin\theta_\mathrm{m})^2}. \tag{4}$$

To aid in understanding the implications of Eqs. (3) and (4), an example circular profile taken about the true center is compared to an equivalent profile taken about an offset center in Fig. 4. Figure 4(a) shows a 10 cycle sinusoidal Siemens star target, with a blue dot showing the correct center of the target ($C_x = C_y = 0$) and a red dot showing an offset center in the $\pi/4$ direction ($C_x/r_\mathrm{m} = C_y/r_\mathrm{m} = 0.1$). The intensity patterns extracted in the polar coordinate system by the correct (blue) and offset (red) centered circles are shown in Fig. 4(b), where phase misalignment of the profile from the offset center appears to be greatest at the angles orthogonal to the offset angle of $\pi/4$. This misalignment is also apparent in Fig. 4(c), where the extracted profiles are more clearly shown as a function of θ_m. Figure 4(d)

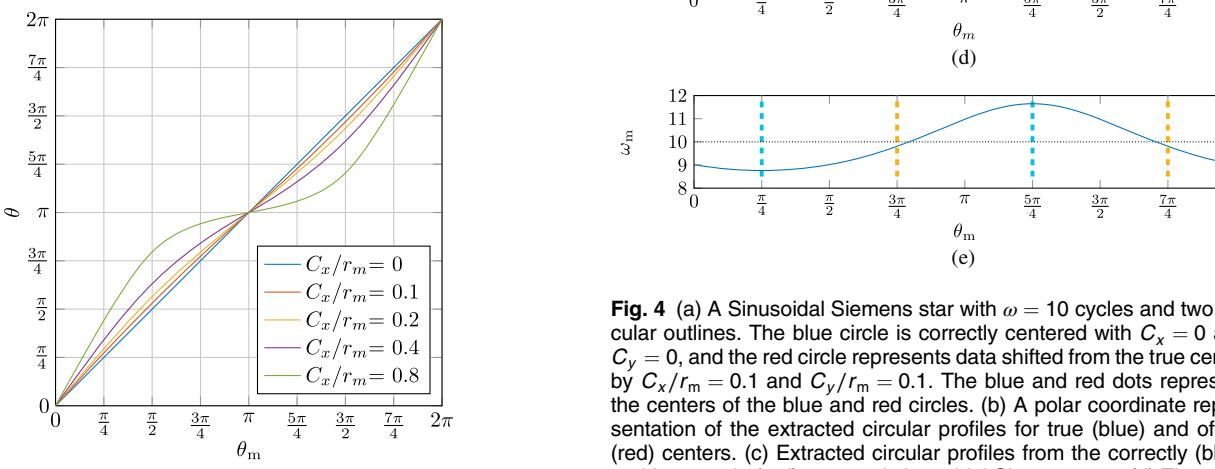

Fig. 3 The relationship between θ and θ_m as a function of C_x/r_m offsets. Note that increasing the offset or decreasing the sampled radius will increase the difference between θ and θ_m.

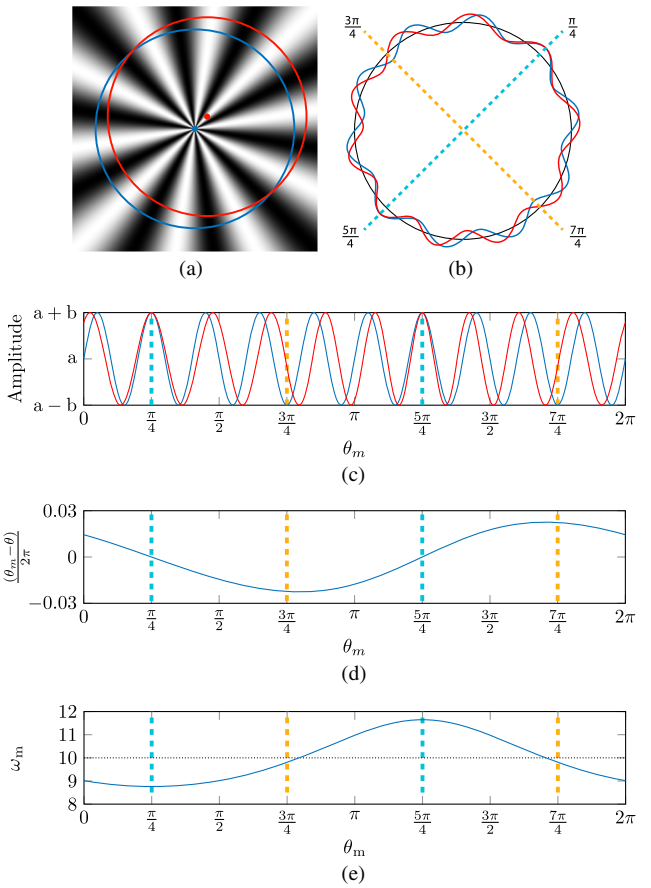

Fig. 4 (a) A Sinusoidal Siemens star with $\omega = 10$ cycles and two circular outlines. The blue circle is correctly centered with $C_x = 0$ and $C_y = 0$, and the red circle represents data shifted from the true center by $C_x/r_\mathrm{m} = 0.1$ and $C_y/r_\mathrm{m} = 0.1$. The blue and red dots represent the centers of the blue and red circles. (b) A polar coordinate representation of the extracted circular profiles for true (blue) and offset (red) centers. (c) Extracted circular profiles from the correctly (blue) and incorrectly (red) centered sinusoidal Siemens star. (d) The error in the polar angle induced by the offset center. (e) The change in the angular frequency (number of target cycles) induced by the offset center.

highlights this error in the polar angle, showing θ_m versus the difference of θ_{m} and θ.

Supporting the initial observation of profile misalignment, the phase angle error for this offset center is near zero in the angles aligned with and opposed to the offset direction, and the largest absolute error is near the angles orthogonal to the offset direction. Interestingly, the error caused by the one cycle modulation of the phase angle does not directly translate to the effective spatial frequency. Figure 4(e) shows that ω_{e} of the profile from the offset center is most different from the true ω of the target in the directions aligned with and opposed to the offset direction.

This difference in the frequency of the extracted profile has significant implications when assuming a known angular frequency for calculations of the image contrast at that known frequency. While this effect may at first seem innocuous, problems arise when fitting a pure sinusoidal function to Eq. (3), a function with an effective frequency modulation. The ISO 12233 standard recommends extracting a circular profile from an image and performing a least squares fit of the intensity signal with a sine function.

Figure 5 shows the best fit amplitude for a correctly centered, 72 cycle sinusoidal Siemens star for a range of spatial frequencies (i.e., a range of radii), and the best fit amplitude for an incorrectly centered target with a center offset of $(C_x, C_y) = (1\ \mathrm{px}, 0\ \mathrm{px})$. Significant degradation is possible in this ideal case, with decreases in best fit amplitude at all spatial frequencies, and the introduction of contrast inversions at higher frequencies.

3.2 *Simulated Images*

To examine these effects in a more realistic setting, an 8-bit image of a sinusoidal Siemens star was generated mathematically, convolved with a known point spread function (PSF) to simulate an optical aberration, and SFR data was collected by fitting different radial profiles with Eq. (1). A Dirac delta function was chosen to further examine an optically perfect simulated sinusoidal Siemens star, and a nearly diffraction limited Cooke triplet PSF, simulated within Zemax optical design software, was chosen to examine how offset centers affect a realistic, optically degraded image.

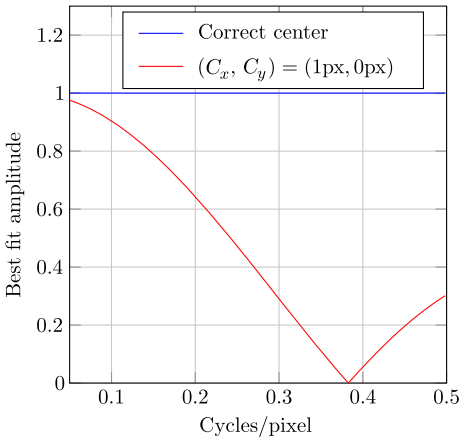

Fig. 5 Spatial frequency response (SFR) extracted from a least squares best fit of Eq. (1) for a correctly centered sinusoidal Siemens star, and an SFR measured for a center offset of $(C_x, C_y) = (1\ \mathrm{px}, 0\ \mathrm{px})$. The sinusoidal Siemens star target has $\omega = 72$ cycles, and a $\phi = 0$.

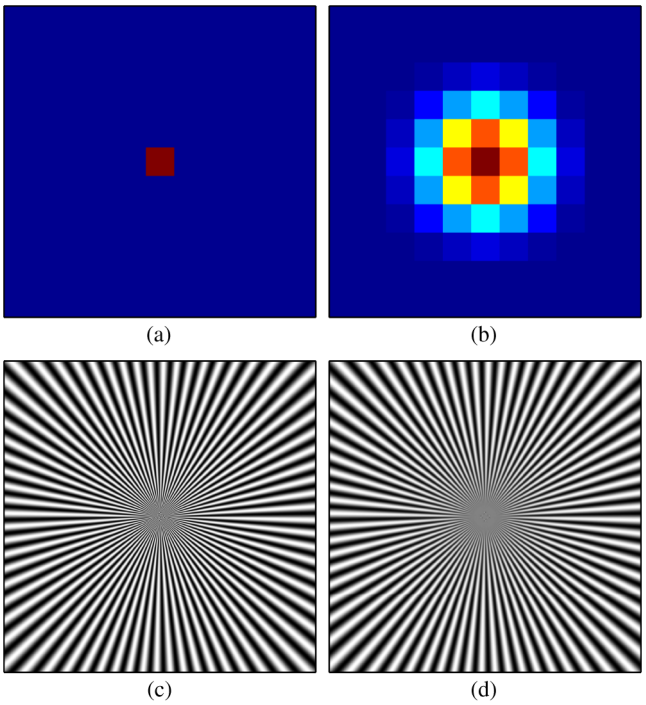

Fig. 6 Discrete point spread functions (PSFs) of: (a) a delta function, (b) a nearly diffraction limited Cooke triplet lens system, (c) and (d) the sinusoidal Siemens star after convolution with the PSFs from (a) and (b), respectively.

The PSFs and sinusoidal Siemens stars convolved with each PSF are shown in Fig. 6. The true center location of each image is known in the generation of these images. We again choose to fit data to the entire radial profile (i.e., one segment is used for the analysis in this subsection). This was chosen so that a comparison could be made between the purely mathematical analysis of Sec. 3.1, and the more realistic case of processing an image of a sinusoidal Siemens star target.

Figure 7 shows best fit contrast (i.e., SFR) versus cycles per pixel for the two PSFs shown in Fig. 6 and with an increasing pixel offset value. Also shown is the area under curve (AUC) for each pixel offset, normalized by the zero-offset center AUC. Examining Fig. 7(a) for a pixel offset of 1 shows a curve that is nearly equivalent to the purely mathematical analysis in Fig. 5, showing differences only due to sampling of the simulated image. In Fig. 7(c), SFR measurements from the Cooke triplet PSF show less degradation for the same pixel offset compared to the Dirac PSF. This is due to realistic optical systems typically yielding low-contrast values at high frequencies, which effectively attenuates the potential errors due to incorrect center locations. However, a single pixel shift reduces the AUC by approximately 17% for the Cooke PSF example.

3.3 *Error Mitigation Through Angular Segmentation*

The ISO 12233 standard states an image of a sinusoidal Siemens star target should be angularly divided into a user defined number of segments, typically eight segments, though 24 segments are mentioned later in the document. Segmentation is stated as a technique derived to assist the processing of distorted images without requiring modifications to the original image. However, angular segmentation

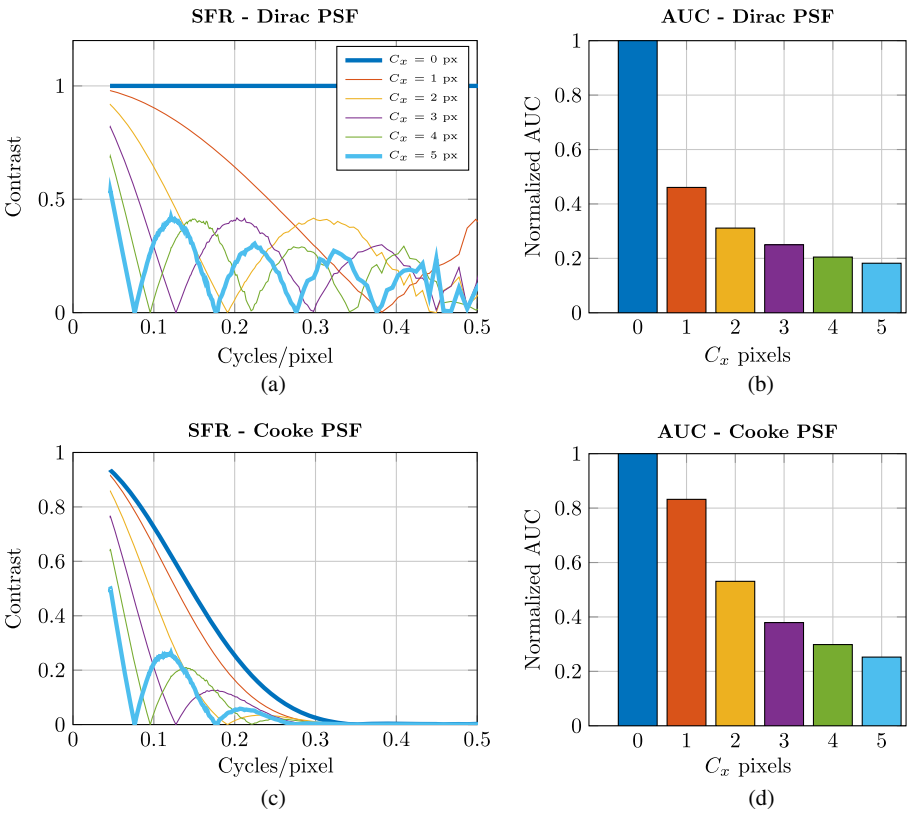

Fig. 7 (a) The measured contrast for a perfect (i.e., Dirac PSF convolved) sinusoidal Siemens star with an increasing center offset error. (b) The AUC measured for (a) from each center offset error, normalized to the correctly centered AUC value. (c) Measured contrast from a sinusoidal Siemens star convolved with a realistic Cooke triplet point spread function. (d) The normalized AUC measured for each offset error from (c).

can also serve the secondary purpose of minimizing errors in the SFR associated with incorrectly determined centers. Conceptually, an offset center can be thought of as generating a nonuniform modulation of the measured signal, as defined by Eq. (3), similar to that of optical distortion. In this subsection we investigate the effect of angular segmentation of data on the normalized AUC given an image with an offset center, and the minimum number of segments needed to reach at least 95% of the nominal AUC.

An image of a 144-cycle sinusoidal Siemens star was analyzed by performing a least squares fit given an offset center ranging from 1 to 10 pixels, in 1 pixel increments, and analyzing the sinusoidal Siemens star in angular segments ranging from 1 to 72 segments. The best fit contrast was averaged over all segments, integrated, and compared to the AUC from the correctly determined center case. The AUC for the zero-offset center is referred to as the nominal AUC. Figure 8 shows the results of this analysis given the previous two PSFs convolved with images of a sinusoidal Siemens star in Fig. 6.

Normalized AUC increases as more segments are used to analyze a sinusoidal Siemens star image, regardless of the level of aberration present in the optical system, and larger offset centers require increased segmentation to reduce errors. To achieve a 95% AUC measurement, the number of segments needed scales approximately linearly with the magnitude of the offset center error. The Dirac PSF convolved image requires more segments than the Cooke PSF convolved image, but both have approximately linear relationships between the number of segments needed to attain 95% AUC and pixel offset. Higher quality optical systems are more influenced by offset centers, as shown in the Dirac PSF case, and require approximately 22 segments to achieve 95% of the nominal AUC for a 3-pixel offset case. The realistic optical aberration of the Cooke PSF convolved image requires at least 10 segments to achieve 95% of the AUC of the nominal case for a 3-pixel offset. Note that the maximum shift, $C_x = 10$, is only 2.22% of the largest radial sample used to analyze this image.

Repeating the analysis above, but for a 72 cycle sinusoidal Siemens star target, shows the Dirac PSF image requires half the number of segments compared to the 144-cycle sinusoidal Siemens star to achieve the same 95% nominal AUC given a 3-pixel center offset. Using the Cooke PSF, maintaining a 95% nominal AUC enables an approximate 15% reduction in the number of segments required compared to the 144-cycle sinusoidal Siemens star. This analysis appears to indicate that a more complex relationship exists between required segments and target cycles.

Based on the assumption that the center of the sinusoidal Siemens star target is found within 3 pixels, using 22 segments appears to minimize errors induced by incorrectly determined centers. However, if an error of greater than 3 pixels is expected from the center finding algorithm, the appropriate number of segments should be increased to reduce error.

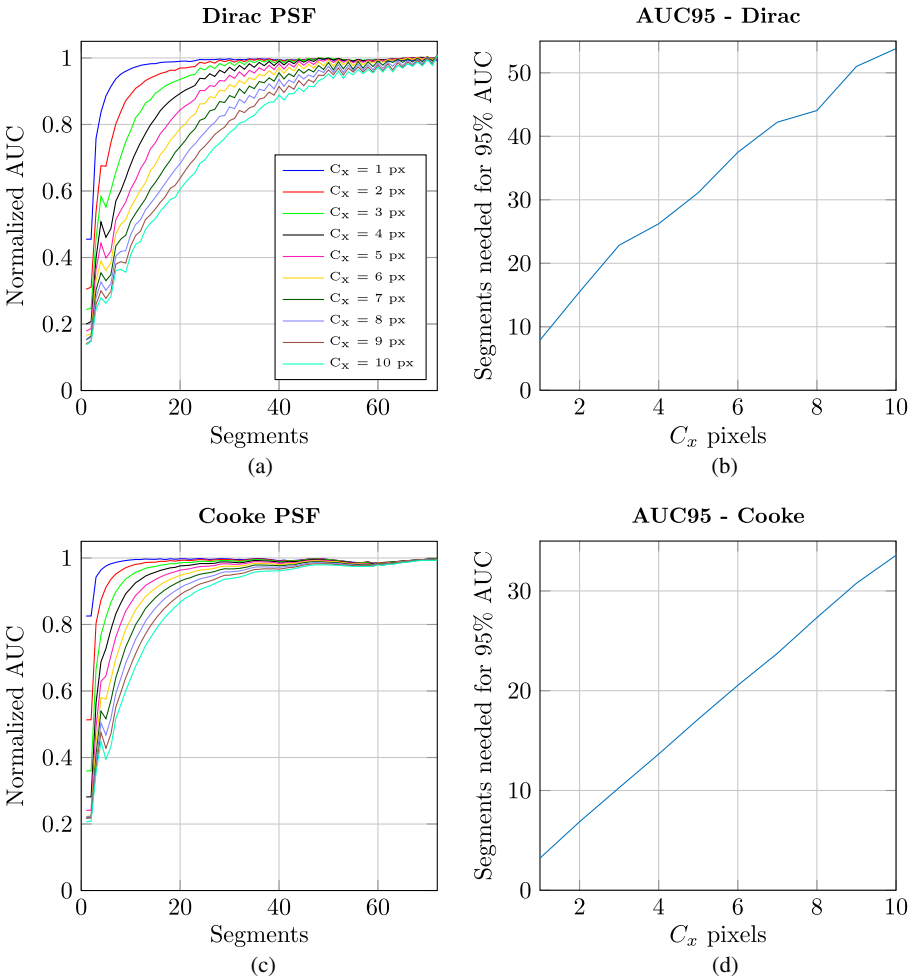

Fig. 8 (a) Normalized AUC versus segments for a Dirac PSF convolved target. (b) Segments needed to maintain 95% nominal AUC for the Dirac PSF convolved target. (c) Normalized AUC versus segments using the Cooke PSF convolved target. (d) Segments needed to maintain 95% nominal AUC using the Cooke PSF convolved target. Test target images are the same used in the analysis discussed in Fig. 7, and used a 144-cycle sinusoidal Siemens star target. These results show that a significant number of segments must be used when the test target center is not correctly identified. Small shifts can yield large decreases in AUC if the appropriate number of segments is not utilized in the SFR analysis.

3.4 *Mitigation Through Proper Location of Target Center*

Regardless of the level of aberration or number of segments used in analysis, an accurate determination of the true center reduces error. We propose a two-step method whereby an initial coarse estimate is made of the center of the target, a low-frequency single circular profile is extracted from the image of the sinusoidal Siemens star, fit to Eq. (3), and constants C_x and C_y are solved for and used to correct the initial guess. A singular circular profile, as visualized in Fig. 4(a), will exhibit a changing spatial frequency dependent upon the magnitude of the center offset error. By extracting this singular circular profile and fitting Eq. 3, the center offsets can be measured.

A Monte-Carlo simulation using 10,000 iterations was performed, where each iteration of the simulation generated an incorrect pixel offset, chosen via Gaussian weighted random number generation using $(\sigma_x, \sigma_y) = (2\text{ px}, 2\text{ px})$. Values were centered about the true center of the test target (i.e., $\mu = 0$). The simulated image parameters used for the Cooke triplet PSF analysis in Sec. 3.2 were reused. Figure 9 shows the offset center locations in red and the corrected center locations in blue after the two-step correction has been applied. After correction, the mean center error is 0.026 pixels, with a standard deviation of 0.014 pixels.

The results from corrected center locations are compared to the results without correction by computing the normalized AUC as a function of pixel offset magnitude. Figure 10 shows these results given a single segment analysis and an eight segment analysis, identified by the ISO 12233 standard as the typical segmentation number. Using one segment fitting and the two-step center estimating process, the maximum relative error compared to the nominal AUC is 0.136%, and the maximum deviation from the true SFR at any spatial frequency is 0.37%. Similar results are seen when eight segments are used, with the maximum relative error compared to the nominal AUC being 0.026%, and the maximum deviation from the true SFR at any spatial frequency being 0.39%. These results clearly show the benefits of using a two-step center finding method. An additional point to note is that the number of segments can be reduced if confidence is sustained in the accuracy of the center finding algorithm.

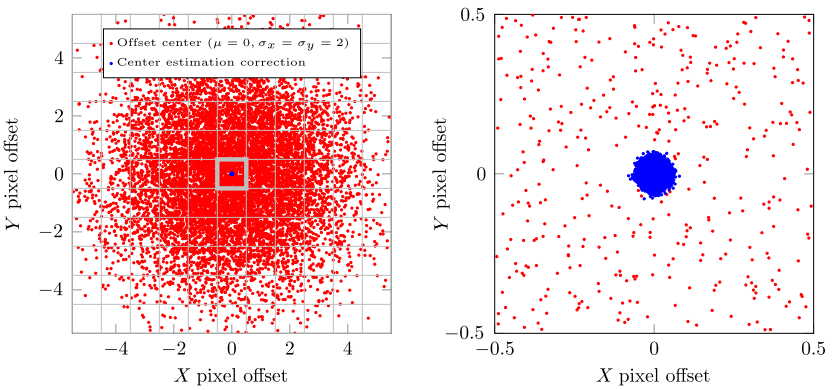

Fig. 9 Offset centers (subpixel) compared to the center of the target, defined as the origin, with red points as the offsets from the Monte-Carlo simulation, and blue points the corrected offsets after applying a least squares fit of Eq. (3) to a single circular profile. Pixels are represented by the grid, and a view of the center pixel is shown on the right.

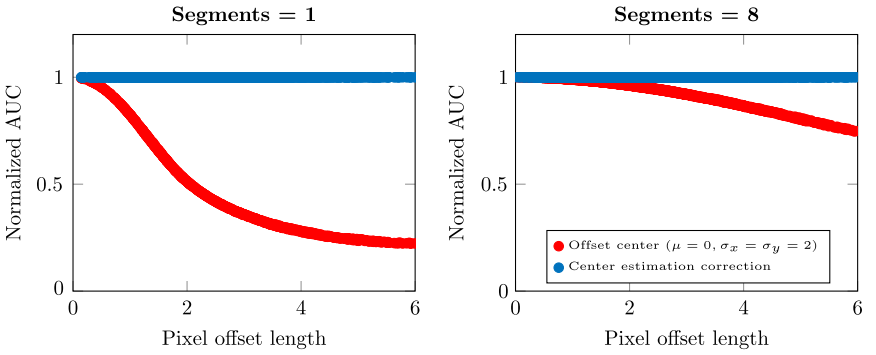

Fig. 10 Normalized AUC versus pixel offset magnitude. The red data shows normalized AUC using a single center estimation step that contains some error and no center correction feedback process, while the blue data shows the results from the proposed two-step center correction method.

3.5 *Analysis of a Real Image*

The previous examples have utilized images created from the mathematical definition of a sinusoidal Siemens star test target, as shown in Eq. (1). A similar analysis is performed using a real image of an ISO 12233:2014 compliant 144-cycle sinusoidal Siemens star test target taken with a Cannon EOS 5D Mark III digital camera. The image of the test target used in this analysis is shown in Fig. 11(a). The center of the test target is found via human analysis. An error of 10 pixels in the x-direction is then added to the true center value, and SFR is measured using 8 segments. Using the techniques described in Sec. 3.4, the incorrect center is mitigated and

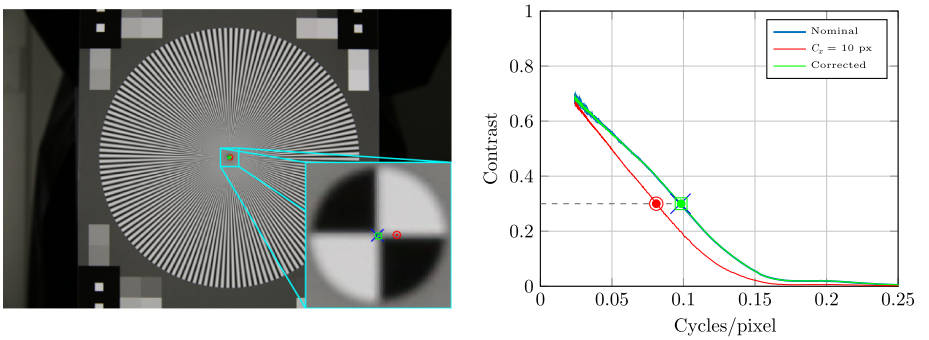

(a) (b)

Fig. 11 (a) Real image taken of an ISO 12233:2014 compliant sinusoidal Siemens star target using a digital camera. The blue x denotes the true center of the test target, as determined by human analysis. The red circle and dot denote a user added error of 10 pixels in the x-direction. The green square and dot represent the corrected center using the technique described in Sec. 3.4. (b) Measured SFR for the nominal, correctly centered case (blue), offset center case (red), and corrected case (green). The dashed line shows the SFR10 value. The red circle and dot, green square and dot, and blue x show the SFR10 values for the offset center measurement, corrected center measurement, and nominal case, respectively.

the SFR is calculated for this corrected case. Figure 11(b) shows the SFR for the nominal, uncorrected, and corrected cases. Before correction, the AUC is 21% less than the nominal AUC, and the spatial frequency measured with 30% contrast, called the SFR30, is 17.3% less than the nominal SFR30. After correction, the AUC is 0.15% greater than the nominal AUC, and the SFR30 value is 0.43% greater than the nominal SFR30.

4 Summary and Future Work

Determining the center of a sinusoidal Siemens star test target image can have significant impact on the SFR extracted from the image. We define an equation that produces the sampled radial profile measured given an incorrectly centered sinusoidal Siemens star. Using this equation we show that significant errors in SFR measurements can occur. Given an image generated using the mathematical definition of a sinusoidal Siemens star target and convolved with a realistic optical PSF, even a single pixel shift and single segment analysis can yield a 17% reduction in the measured AUC compared to the correctly centered nominal AUC. The importance of using enough segments is explored, and the use of additional segments is shown to mitigate errors associated with offset centers. The effect of segmentation, typically used as a method to minimize processing needed to work with distorted images, can decrease the error in the calculated SFR produced by an offset center. However, just a few pixels offset in the center location require more than eight segments, which is the number stated to be a typical user-defined value by the ISO 12233 standard. A two-step process is defined that first takes an initial coarse estimate of the target center, then extracts a single circular profile in order to calculate the location of the true center based on Eq. (3). Monte-Carlo simulation results show that regardless of the magnitude of the center offset, or of the numbers of segments used, the two-step center correction process enables more precise calculation of the SFR compared to the true, correctly centered measurement. Finally, the two-step center correction process is demonstrated using an image of a sinusoidal Siemens star target taken with a digital camera.

There are several areas that would benefit from further investigation. A deeper relationship between the offset center, cycles per target, and aberration content appears to exist and merits further exploration. Furthermore, an error analysis of techniques used to mitigate errors due to distortion would be useful.

We conclude by stating that care must be taken when identifying the center of a sinusoidal Siemens star. This report shows that error will be intrinsically present in the SFR results of this test if the center is not correctly identified.

Acknowledgments

Sandia National Laboratories is a multiprogram laboratory managed and operated by Sandia Corporation, a wholly owned subsidiary of Lockheed Martin Corporation, for the U.S. Department of Energy's National Nuclear Security Administration under contract DE-AC04-94AL85000. SAND2015-3823 J.

References

1. ISO for Standardization. Technical Committee Photography, *ISO-12233:2014–Photography: Electronic Still-Picture Cameras–Resolution Measurements*, ISO (2014).
2. U. Artmann and D. Wueller, "Differences of digital camera resolution metrology to describe noise reduction artifacts," *Proc. SPIE* **7529**, 75290L (2010).
3. C. Loebich et al., "Digital camera resolution measurement using sinusoidal siemens stars," *Proc. SPIE* **6502**, 65020N (2007).
4. T. W. Du Bosq, D. P. Haefner, and B. L. Preece, "Performance assessment of compressive sensing imaging," *Proc. SPIE* **9071**, 90710G (2014).
5. V.-T. Peltoketo, "Evaluation of mobile phone camera benchmarking using objective camera speed and image quality metrics," *J. Electron. Imaging* **23**(6), 061102 (2014).
6. K. Atanassov and S. Goma, "Evaluating the quality of EDOF in camera phones," *Proc. SPIE* **7529**, 75290K (2010).
7. D. Do, H. Yoo, and D.-G. Gweon, "Fiber-optic raster scanning two-photon endomicroscope using a tubular piezoelectric actuator," *J. Biomed. Opt.* **19**(6), 066010 (2014).
8. S. Rupp, "A quantitative performance measure for a clinical evaluation of comb structure removal algorithms in flexible endoscopy," *Proc. SPIE* **6914**, 69141C (2008).
9. A. Weckenmann et al., "Practice-oriented evaluation of lateral resolution for micro- and nanometre measurement techniques," *Meas. Sci. Technol.* **20**(6), 065103 (2009).
10. L. Cao and J. Peter, "Iterative reconstruction of projection images from a microlens-based optical detector," *Opt. Express* **19**, 11932–11943 (2011).
11. Y. Duan et al., "Design and experiment of uav remote sensing optical targets," in *2011 Int. Conf. on Electronics, Communications and Control (ICECC)*, pp. 202–205 (2011).
12. D. Wueller, "Evaluating digital cameras," *Proc. SPIE* **6069**, 60690K (2006).

Gabriel C. Birch is a research scientist at Sandia National Laboratories. He received his PhD in optical sciences from the University of Arizona College of Optical Sciences in 2012. His current research interests include physical security systems, testing and evaluation of imaging devices, and nontraditional imaging systems.

John C. Griffin is a research scientist at Sandia National Laboratories, where he pursues interests in data analysis, instrumentation, and optimization. He received his PhD in mechanical engineering from the University of Florida, where he focused on flow control using reduced-order models.